

PAPER • OPEN ACCESS

## Non-Hermitian topological states in 2D line-graph lattices: evolving triple exceptional points on reciprocal line graphs

To cite this article: Hang Liu *et al* 2021 *New J. Phys.* **23** 123038

View the [article online](#) for updates and enhancements.

You may also like

- [Ferromagnetic ground states for the Hubbard model on line graphs](#)  
A Mielke
- [Isospectral graphs with identical nodal counts](#)  
Idan Oren and Ram Band
- [Some physical and chemical indices of clique-inserted lattices](#)  
Zuhe Zhang



## PAPER

Non-Hermitian topological states in 2D line-graph lattices:  
evolving triple exceptional points on reciprocal line graphs

## OPEN ACCESS

RECEIVED  
17 August 2021REVISED  
29 October 2021ACCEPTED FOR PUBLICATION  
7 December 2021PUBLISHED  
22 December 2021Original content from  
this work may be used  
under the terms of the  
[Creative Commons  
Attribution 4.0 licence](#).Any further distribution  
of this work must  
maintain attribution to  
the author(s) and the  
title of the work, journal  
citation and DOI.Hang Liu<sup>1,2,3</sup> , Sheng Meng<sup>2,3,\*</sup> and Feng Liu<sup>1,\*</sup><sup>1</sup> Department of Materials Science and Engineering, University of Utah, Salt Lake City, Utah 84112, United States of America<sup>2</sup> Songshan Lake Materials Laboratory, Dongguan, Guangdong 523808, People's Republic of China<sup>3</sup> Beijing National Laboratory for Condensed Matter Physics and Institute of Physics, Chinese Academy of Sciences, Beijing 100190, People's Republic of China

\* Authors to whom any correspondence should be addressed.

E-mail: [smeng@iphy.ac.cn](mailto:smeng@iphy.ac.cn) and [fliu@eng.utah.edu](mailto:fliu@eng.utah.edu)**Keywords:** exceptional point, line graph, non-Hermitian systems, topological statesSupplementary material for this article is available [online](#)**Abstract**

Non-Hermitian (NH) topological states, such as the doubly-degenerate nodes dubbed as exceptional points (EPs) in Bloch band structure of 2D lattices driven by gain and loss, have attracted much recent interest. We demonstrate theoretically that in the three-site edge-centered lattices, i.e. the so-called line-graph lattices, such as kagome lattice which is a line graph of hexagonal lattice, there exist three types of triply-degenerate EPs evolving intriguingly on another set of line graphs in the reciprocal space. A single TEP (STEP) with  $\pm 1/3$  topological charge moves faithfully along the edges of reciprocal line graphs with varying gain and loss, while two STEPs merge distinctively into one unconventional orthogonal double TEP (DTEP) with  $\pm 2/3$  charge at the vertices, which is characterized with two ordinary self-orthogonal eigenfunctions but one surprising 'orthogonal' eigenfunction. Differently, in a modified line-graph lattice with an off-edge-center site, the ordinary coalesced state of DTEPs emerges with three identical self-orthogonal eigenfunctions. Such NH states and their evolution can be generally realized in various artificial systems, such as photonic and sonic crystals, where light and sonic vortex beams with different fractional twisting can be found. Our findings shed new light on fundamental understanding of gapless topological states in NH systems in terms of creation and evolution of high-order EPs, and open up new research directions to further link line graph and flow network theory coupled with topological physics, especially under non-equilibrium gain/loss conditions.

**1. Introduction**

Non-Hermitian (NH) lattices with onsite gain and loss have been shown to exhibit various topological phenomena. For example, in a rhombic lattice under driving, a Dirac point splits into a pair of doubly-degenerate exceptional points (EPs), each characterized with degenerate eigenvalues and identical self-orthogonal eigenvectors [1–7]. The topology of an EP is characterized by a nonzero topological invariant

$$\nu = -\frac{1}{2\pi} \oint_{\text{EP}} \nabla_{\mathbf{k}} \arg [E_1(\mathbf{k}) - E_2(\mathbf{k})] \cdot d\mathbf{k} = \pm \frac{1}{2}, \quad (1)$$

where integration is carried out on a  $\mathbf{k}$ -space loop enclosing the EP.  $E_1(\mathbf{k})$  and  $E_2(\mathbf{k})$  are two complex eigenvalues at each  $\mathbf{k}$  point. The invariant represents a winding number, associated with the energy dispersion of NH band structures around the EP, i.e. the vorticity around the EP. The vorticity manifests also a topological charge  $\nu$  with the physical implication of polarization [1]. It has been demonstrated that [2] the nonzero  $\nu$  implies the existence of band degeneracy within the region enclosed by the loop, and an EP with half topological charge  $\nu = \pm 1/2$  can be described by the Riemann surface  $f = z^{1/2}$  ( $z$  is a complex number) with a nodal point being doubly degenerated. A pair of EPs are connected by a bulk Fermi arc

(BFA) with the degenerate real part but nondegenerate imaginary part of eigenvalues [1], which manifests itself in creating vortex beam with fractional charge. The EPs with higher degeneracy are used to create vortex beam beyond  $\pm 1/2$  charge for enhancing sensitivity of NH detectors [8–13]. Other gapless NH topological states include exceptional lines, rings, and surfaces [14–22]. Furthermore, gapped NH topological states have been demonstrated for potential applications in making robust single-color laser based on NH Haldane cavity [23–26]. The second-order NH topological insulators can afford sound guides in sonic crystals [27, 28]. Therefore, imposing non-Hermiticity to a Hermitian system is an effective way to induce novel topological states, which is of both scientific and technological interests.

On the other hand, it is well recognized that all the 2D edge-center lattices can be viewed as line-graph lattices, since they can be constructed as line graphs in mathematical graph theory. A line graph is made by connecting the centers of edges that share a common vertex of the original graph. Interestingly, the line-graph lattices have been shown to exhibit exotic properties associated with topology and many-body interactions, such as magnetism and superconductivity [29–32]. One prevailing theorem is that the topological construction of line graph underlines a necessary condition for the existence of topological flat bands in the line-graph lattices, such as the well-known kagome lattice, where destructive interference of lattice wavefunctions leads to formation of highly localized compact plaquette quantum states [33, 34]. Then, an intriguing question arises: what happens when non-Hermiticity is introduced in the line-graph lattices? How the band topology will evolve with gain and loss, especially noting that an NH line graph may be linked to a non-equilibrium flow network in graph theory.

In this article, the band structure and topology of a class of 2D NH line-graph lattices, with three sites having gain and loss, are explored. Most strikingly, three types of triply degenerate EPs (TEPs) are found to always exist on another set of line graphs in the reciprocal space. By continuously varying gain and loss, single TEPs (STEPs) with  $\pm 1/3$  charge move faithfully along the edges of reciprocal line graphs. When two STEP s meet at the vertices of the reciprocal line graph, they merge distinctively into an unconventional orthogonal double TEP (DTEP) with  $\pm 2/3$  charge, featured with two identical ordinary self-orthogonal eigenfunctions but another surprising orthogonal eigenfunction. Differently, in the modified off-center line-graph lattices, in which one of the vertices of line graph is chosen along the edge but at an off-center position of the original graph, an ordinary coalesced state of DTEPs appear at the vertices, with three degenerate eigenvalues and identical self-orthogonal eigenfunctions. The intriguing evolution of TEPs in a reciprocal line graph and the existence of orthogonal DTEP (ODTEP) signify a set of unique NH topological properties of line-graph lattices.

## 2. TEPs in NH kagome lattice

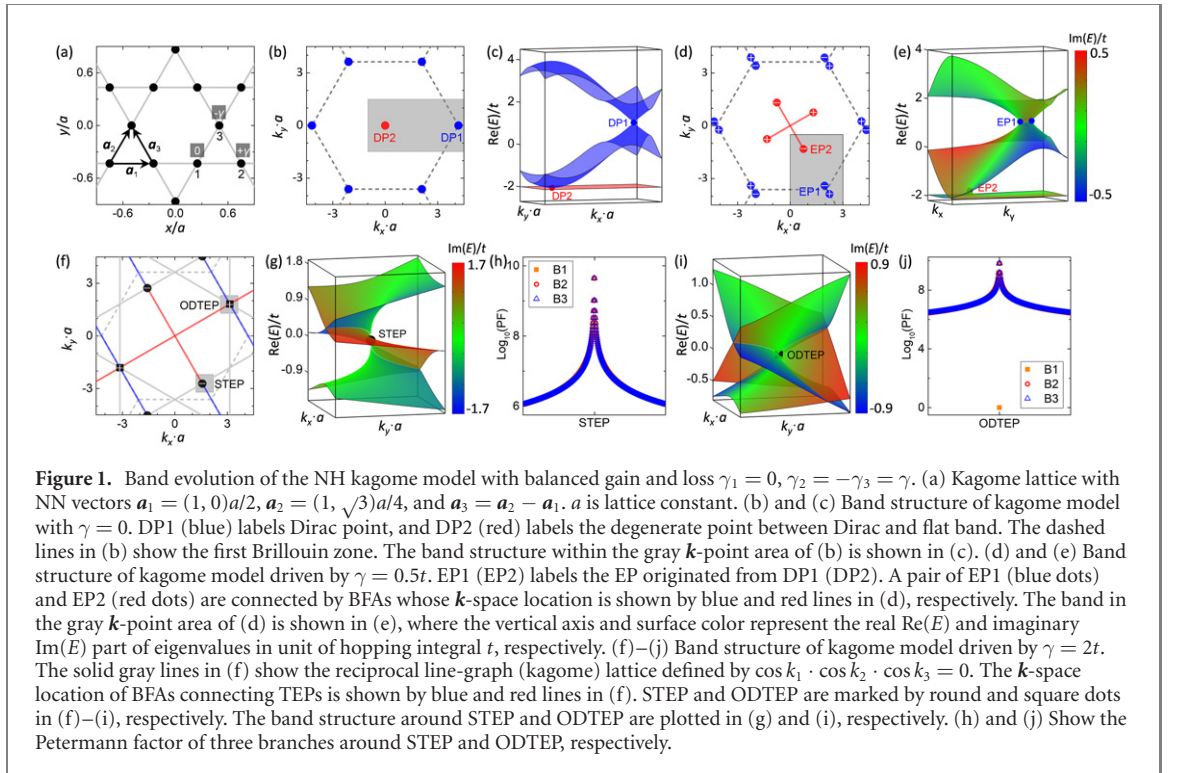
We first consider a kagome lattice with gain and loss  $\gamma_n$  ( $n = 1, 2, 3$ ) at  $n$ th site, as shown in figure 1(a). The NH kagome Hamiltonian is

$$H = 2t \begin{pmatrix} 0 & \cos k_1 & \cos k_2 \\ \cos k_1 & 0 & \cos k_3 \\ \cos k_2 & \cos k_3 & 0 \end{pmatrix} + i \begin{pmatrix} \gamma_1 & 0 & 0 \\ 0 & \gamma_2 & 0 \\ 0 & 0 & \gamma_3 \end{pmatrix}, \quad (2)$$

where  $k_n = \mathbf{k} \cdot \mathbf{a}_n$ , and  $t$  is the nearest-neighbor (NN) hopping integral. The balanced gain and loss  $\gamma_1 = 0$ ,  $\gamma_2 = -\gamma_3 = \gamma$  is adopted to study the evolution of band structure. When  $\gamma = 0$ , the original Hermitian kagome model exhibits two Dirac bands touched with a bottom flat band (figures 1(b) and (c)), where the Dirac (degenerate) point at  $K$  ( $\Gamma$ ) is labeled as DP1 (DP2). As shown in figures 1(d) and (e), when  $\gamma$  increases to  $0.5t$ , DP1 splits into a pair of two-fold EPs (labeled as EP1), whose band shape in low energy can be described by the complex function  $f = z^{1/2}$  containing all topologies of nodal points EP1 (see figure S1 (<https://stacks.iop.org/NJP/23/123038/mmedia>) in supplemental material). The EP1 pair, with a topological charge  $\nu = \pm 1/2$  on each EP (computed by equation (1)), is connected by a BFA with the degenerate real but nondegenerate imaginary part of eigenvalues, which illustrates the nontrivial topology of the EPs. Meanwhile, DP2 splits into four EPs (labeled as EP2) which are connected by two crossing BFAs.

When  $\gamma$  increases further to  $2t$ , EP1 ( $\nu = -1/2$ ) and EP2 ( $\nu = -1/2$ ) merge together to form a TEP node, as shown in figures 1(f)–(h). To distinguish the exceptionality of the TEP node, we calculated the Petermann factor [8, 35]

$$\text{PF}_n = \frac{\langle \psi_n^L | \psi_n^L \rangle \langle \psi_n^R | \psi_n^R \rangle}{|\langle \psi_n^L | \psi_n^R \rangle|^2} \quad (3)$$



for the states with eigenvalues  $E_n$  around the node, where  $n = 1, 2, 3$  is band index. In equation (3), the left eigenfunction  $\langle \psi_n^L |$  and right eigenfunction  $|\psi_n^R\rangle$  are solved from Schrödinger equations  $\langle \psi_n^L | H = \langle \psi_n^L | E_n$  and  $H |\psi_n^R\rangle = E_n |\psi_n^R\rangle$  with the NH Hamiltonian  $H,$  respectively. As shown in figure 1(h), approaching the TEP nodal point, the factors  $\text{PF}_n$  of three energy branches become divergent  $\text{PF}_n \rightarrow +\infty,$  indicating the left and right eigenfunctions are self-orthogonal, i.e.  $\langle \psi_n^L | \psi_n^R \rangle \rightarrow 0.$  The self-orthogonality indicates that the nodal point is an EP with triple degeneracy [8], i.e. STEP. To characterize its topology, we define the winding number (similar to equation (1)) of eigenvalues enclosing the EP as a topological invariant

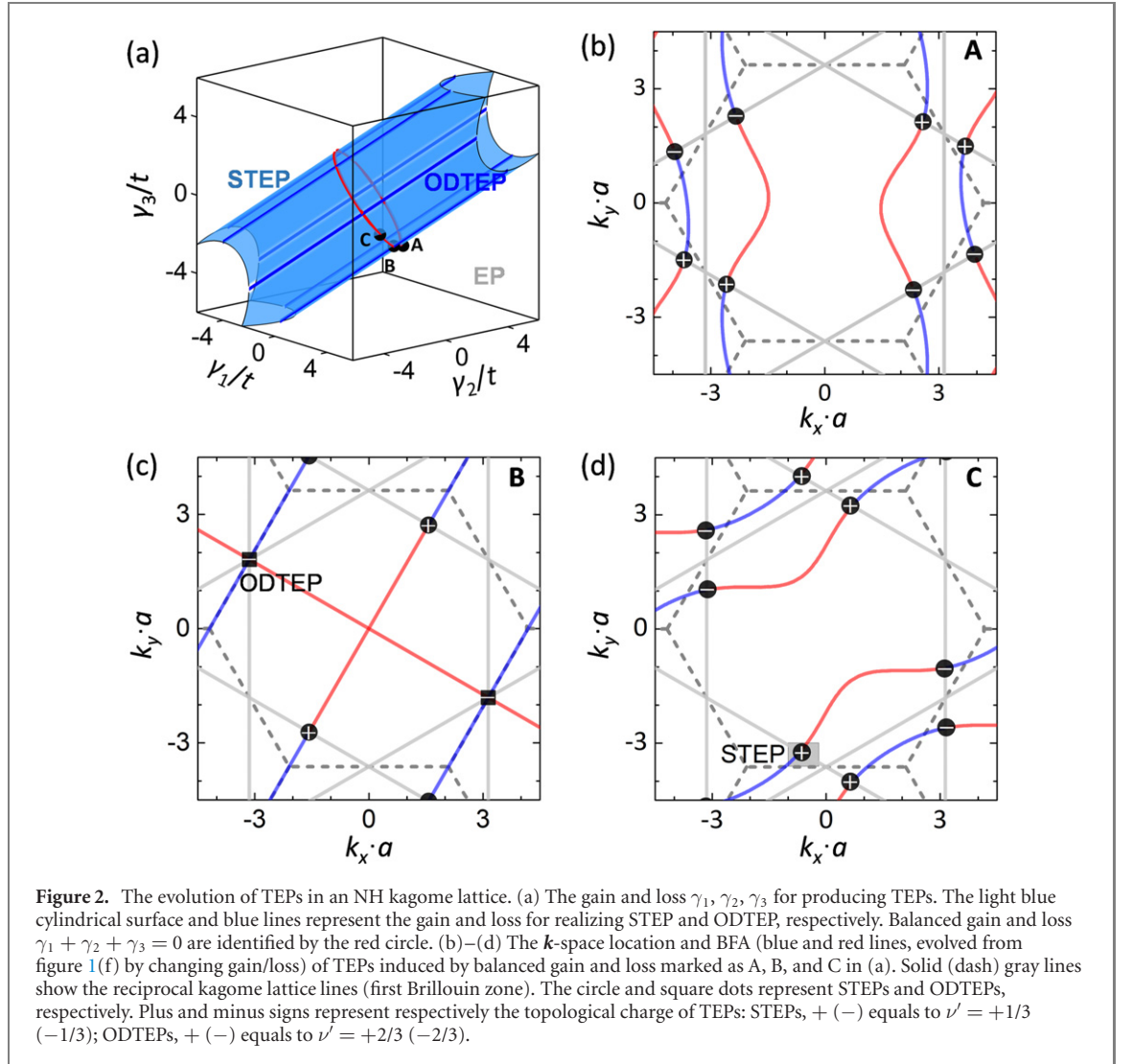
$$\begin{aligned} \nu' = & -\frac{1}{2\pi} \oint_{\text{TEP}} \frac{1}{3} \{ \nabla_{\mathbf{k}} \arg [ +E_1(\mathbf{k}) - E_2(\mathbf{k}) - E_3(\mathbf{k}) ] \\ & + \nabla_{\mathbf{k}} \arg [ -E_1(\mathbf{k}) + E_2(\mathbf{k}) - E_3(\mathbf{k}) ] \\ & + \nabla_{\mathbf{k}} \arg [ -E_1(\mathbf{k}) - E_2(\mathbf{k}) + E_3(\mathbf{k}) ] \} \cdot d\mathbf{k} \end{aligned} \quad (4)$$

The STEP exhibits a fractional topological charge  $\nu' = -1/3,$  consistent with its low-energy band shape described by the complex function  $f = \pm(z^*)^{1/3}.$  The STEPs are connected by two BFAs originating from the degenerate real part of eigenvalues on two lower and higher bands, respectively. Meanwhile, two EP1 ( $\nu = +1/2$ ) and two EP2 ( $\nu = +1/2$ ) merge together at M point, forming a TEP node, as shown in figures 1(f) and (i). The node is found to have a low-energy band shape  $f = \pm z^{2/3}$  and exhibit a topological charge  $\nu' = +2/3$  which is twice of that for an STEP. Approaching the node, all three branches exhibit divergent PF (figure 1(j)), indicating also the node is exceptional (a known signature of EPs [8]). However, although this exceptional nodal point has three degenerate eigenvalues, surprisingly, only two eigenfunctions are found self-orthogonal as expected, while the remaining third eigenfunction is orthogonal to the first two. Given this unusual form of orthogonality and its doubled topological charge, the nodal point is dubbed as ODTEP. Meanwhile, as shown in figure 1(f), the BFAs, which connect all the TEPs, develop into a network, where the ODTEP locates at the nodes of network; the continuous BFAs for high-order TEPs are in sharp contrast to the separate BFAs of doubly-degenerate EPs in figure 1(d).

Next, we study the evolution of TEPs by continuously varying the gain and loss. To create TEPs, the gain and loss should satisfy

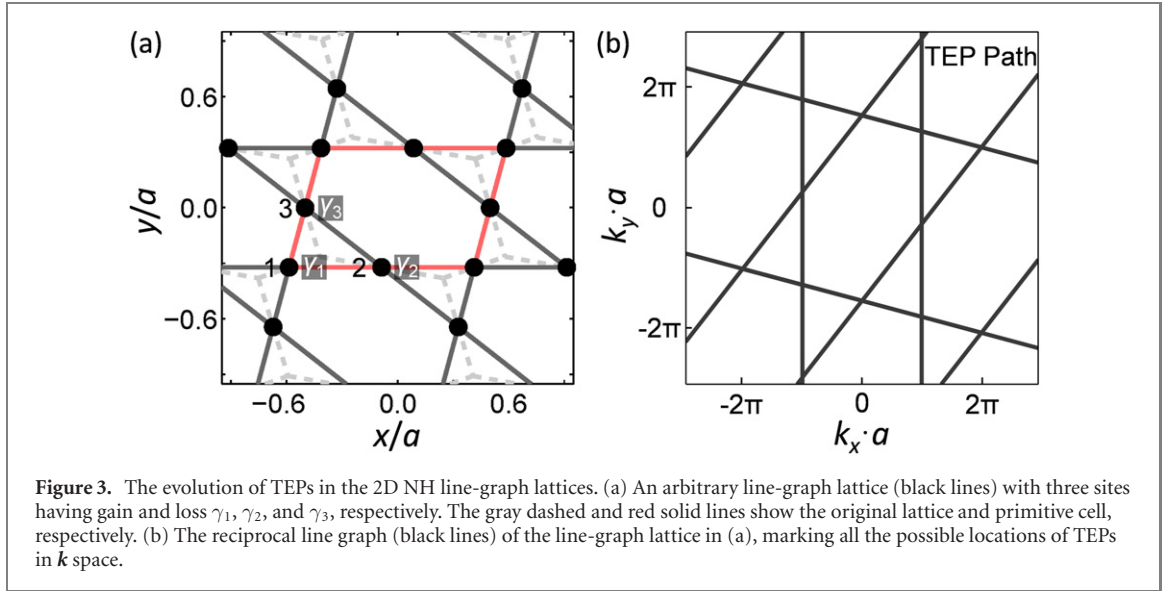
$$12t^2 = (\gamma_1 + \gamma_2 + \gamma_3)^2 - 3(\gamma_1\gamma_2 + \gamma_1\gamma_3 + \gamma_2\gamma_3), \quad (5)$$

as shown by the cylindrical surface in figure 2(a) (see details in supplemental material), in the parameter space of  $\gamma_n.$  We first analyze the case of balanced gain and loss  $\gamma_1 + \gamma_2 + \gamma_3 = 0.$  When the gain and loss follow  $\gamma_1 = t, \gamma_2 = (-1 + \sqrt{15})t/2, \gamma_3 = -(1 + \sqrt{15})t/2,$  there exist STEPs with  $\nu' = +1/3$  ( $-1/3$ ) on



the lines satisfying  $\cos k_2 = 0$  ( $\cos k_3 = 0$ ), where a BFA connects a pair of STEPs with opposite charge, and the BFAs are shaped like curves which are continuous in reciprocal space (figure 2(b)). When the gain and loss are changed to  $\gamma_1 = -\gamma_3 = 2t, \gamma_2 = 0$ , the two STEPs on the lines of  $\cos k_3 = 0$  merge together, forming the ODTEP with  $\nu' = -2/3$  at the sites satisfying  $\cos k_1 = \cos k_3 = 0$ , where the bulk Fermi net (BFN) appears to connect all TEPs with all the ODTEPs located at the nodes of the BFN (figure 2(c)). When the gain and loss are further changed to  $\gamma_1 = 4t/\sqrt{3}, \gamma_2 = \gamma_3 = -2t/\sqrt{3}$ , the ODTEP at  $\cos k_1 = \cos k_3 = 0$  splits into two STEPs along the line satisfying  $\cos k_1 = 0$  (figure 2(d)). Consequently, all the TEPs are connected in the NH kagome lattice, occupying exactly all the positions in another  $\mathbf{k}$ -space kagome lattice, i.e. a line graph in reciprocal space with the edges defined by  $\cos k_1 \cdot \cos k_2 \cdot \cos k_3 = 0$ , that is  $\mathbf{k} \cdot \mathbf{a}_n = \frac{\pi}{2} \cdot (2p + 1)$  with an integer  $p$ .

The unbalanced gain and loss will induce the same type of TEP evolution. To create the ODTEP at reciprocal kagome sites (i.e. vertices of reciprocal line graphs) at  $\cos k_1 = \cos k_2 = 0$  ( $\cos k_1 = \cos k_3 = 0$ ,  $\cos k_2 = \cos k_3 = 0$ ), the required gain and loss is found to be  $\begin{cases} \gamma_2 = \gamma_1 \pm 2t \\ \gamma_3 = \gamma_1 \mp 2t \end{cases}$   $\begin{cases} \gamma_2 = \gamma_1 \pm 2t \\ \gamma_3 = \gamma_1 \pm 4t \end{cases}$ , which are shown by six straight lines on the cylinder in figure 2(a). The rest of gain and loss on the cylinder produces STEPs along the reciprocal kagome lines. Overall, the varying gain and loss according to equation (5) will move the STEPs along the reciprocal kagome lines, and merge two STEPs into one ODTEP at reciprocal kagome sites. Furthermore, if lattice hopping beyond NN is included, this evolution pattern of TEPs remains intact; the only difference is that the reciprocal lattice lines become curved (see figure S2 in supplemental material).



### 3. TEPs in NH line-graph lattices

Next, we investigate whether the above TEPs and corresponding evolution exist in other related 2D crystal lattices. For a general NH Hamiltonian

$$H = \begin{pmatrix} 0 & m_1(\mathbf{k}) & m_2(\mathbf{k}) \\ m_1^*(\mathbf{k}) & 0 & m_3(\mathbf{k}) \\ m_2^*(\mathbf{k}) & m_3^*(\mathbf{k}) & 0 \end{pmatrix} + i \begin{pmatrix} \gamma_1 & 0 & 0 \\ 0 & \gamma_2 & 0 \\ 0 & 0 & \gamma_3 \end{pmatrix}, \quad (6)$$

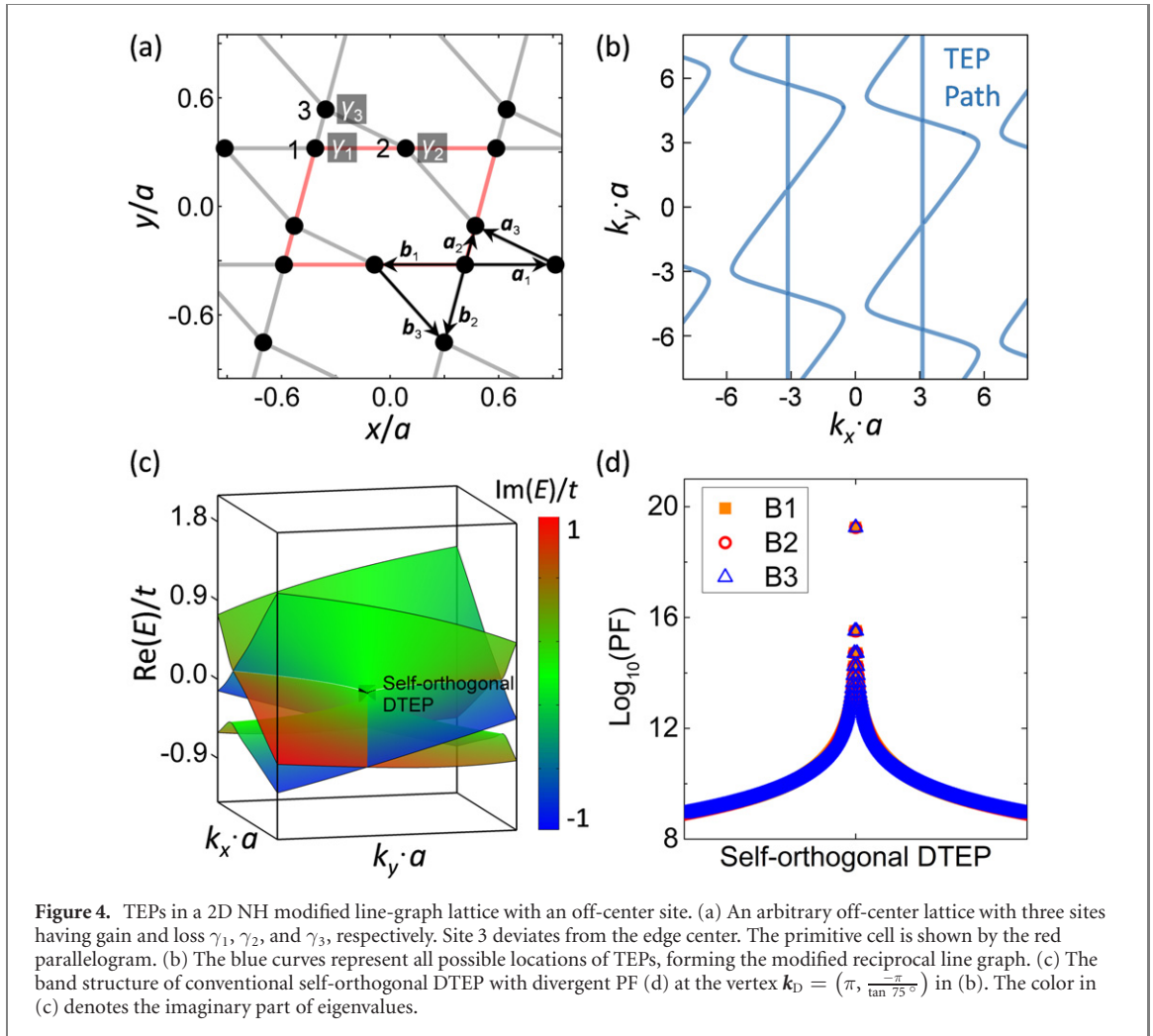
to have a TEP eigenvalue, the condition  $\text{Re}(m_1 m_2^* m_3) = 0$  should be satisfied (see the derivation and figure S3 in supplemental material); meanwhile, the balanced gain and loss must satisfy  $\gamma_1 \gamma_2 + \gamma_1 \gamma_3 + \gamma_2 \gamma_3 + |m_1|^2 + |m_2|^2 + |m_3|^2 = 0$ , and  $\gamma_1 |m_3|^2 + \gamma_2 |m_2|^2 + \gamma_3 |m_1|^2 + \gamma_1 \gamma_2 \gamma_3 = 0$ . Similar to the TEPs satisfying  $\cos k_1 \cdot \cos k_2 \cdot \cos k_3 = 0$  in the kagome lattice, for the three eigenvalues to stay along the reciprocal lattice lines in  $\mathbf{k}$  space, the relation  $\text{Re}(m_1 m_2^* m_3) \propto \cos k_1 \cdot \cos k_2 \cdot \cos k_3$  is required, which has an obvious solution of  $m_1 \propto \cos k_1, m_2 \propto \cos k_2,$  and  $m_3 \propto \cos k_3$ . This indicates that the lattice is generally a line graph of any hexagonal parallelogons (hexagons with parallel sides), which represents actually an edge-center lattice, in which  $m_1 = 2t_1 \cos k_1, m_2 = 2t_2 \cos k_2$  and  $m_3 = 2t_3 \cos k_3$ , with hopping integrals  $t_1 (t_2, t_3)$  between site 1 and 2 (1 and 3, 2 and 3), as shown in figure 3(a). Thus, all the line-graph lattices with gain and loss, at least of this class, support TEPs which are located on another reciprocal line graph in  $\mathbf{k}$  space (figure 3(b)). Varying gain and loss will effectively induce a transition from one ODTEP at a reciprocal line-graph lattice site to two STEPs on the neighboring reciprocal lattice lines, and vice versa.

Next, to further examine the robustness of the above line-graph TEPs, we relax the condition of constructing line graphs. A change is made to construct a modified line-graph 2D lattice with one off-center site: instead of choosing edge centers of the original graph as vertices of the line graph, we choose some off-edge-center points as the vertices, to form a 2D lattice with one site deviating from the center of ‘edge’, as shown in figure 4(a). The vectors between NN sites are  $\mathbf{b}_1 = -\mathbf{a}_1, \mathbf{b}_2 \neq -\mathbf{a}_2,$  and  $\mathbf{b}_3 \neq -\mathbf{a}_3$ , and the corresponding Hamiltonian is

$$H = \begin{pmatrix} 0 & 2t_1 \cos k_1 & t_2 e^{ik_2} + t_2' e^{ik_2'} \\ 2t_1 \cos k_1 & 0 & t_3 e^{ik_3} + t_3' e^{ik_3'} \\ t_2 e^{-ik_2} + t_2' e^{-ik_2'} & t_3 e^{-ik_3} + t_3' e^{-ik_3'} & 0 \end{pmatrix} + i \begin{pmatrix} \gamma_1 & 0 & 0 \\ 0 & \gamma_2 & 0 \\ 0 & 0 & \gamma_3 \end{pmatrix}, \quad (7)$$

where  $k_n = \mathbf{k} \cdot \mathbf{a}_n, k_n' = \mathbf{k} \cdot \mathbf{b}_n,$  and  $t_n (t_n')$  is hopping integral along  $\mathbf{a}_n (\mathbf{b}_n)$ . Based on  $\text{Re}(m_1 m_2^* m_3) = 0$ , the presence of TEPs requires  $\text{Re} \left[ (2t_1 \cos k_1) (t_2 e^{-ik_2} + t_2' e^{-ik_2'}) (t_3 e^{ik_3} + t_3' e^{ik_3'}) \right] = 0$ , which depends on hopping integrals.

To show TEPs, a specific model is arbitrarily chosen with lattice vectors  $\mathbf{a} = (1, 0)a,$   $\mathbf{b} = \frac{2}{3} (\cos 75^\circ, \sin 75^\circ) a$  and the NN vector  $\mathbf{b}_2 = -2\mathbf{a}_2,$  and hopping integrals have an exponential decay with distance  $t_n = t_1 \exp\left(\frac{|a_1| - |a_n|}{|a_1|}\right)$ . STEPs are found to exist on the  $\mathbf{k}$ -space lines satisfying  $\cos k_1 = 0,$  or  $\text{Re} \left[ (t_2 e^{-ik_2} + t_2' e^{-ik_2'}) (t_3 e^{ik_3} + t_3' e^{ik_3'}) \right] = 0$ . Compared with reciprocal line-graph TEP paths in NH



line-graph lattices (figure 3(b)), the TEP path here is modified due to the off-center position for one of the lattice sites (figure 4(b)), which breaks down the intersection condition of  $\cos k_2 = \cos k_3 = 0$ , preventing two STEPs from merging into one ODTEP. Other crossing points along the TEP paths still exist to support DTEPs, which are located at the sites satisfying  $k_x = (2q + 1)\pi$ , and  $k_y = \frac{(3-4 \cos 75^\circ)k_x + 3(2p+1)\pi}{4 \sin 75^\circ}$  with integers  $p$  and  $q$ . As an example, a specific gain and loss is applied to create the DTEP at  $\mathbf{k}_D = (\pi, \frac{-\pi}{\tan 75^\circ})$ , as shown in figures 4(c) and (d). The PF of three branches becomes divergent when approaching the  $\mathbf{k}_D$  point. Most noticeably, different from that in NH line-graph lattices, all three states associated with two merged STEPs are self-orthogonal, showing an ordinary coalesced state of eigenfunctions. The resulting nodal point has also a topological charge  $\nu' = \pm 2/3$ . Thus, it is actually a conventional self-ODTEP. One finds that although a perfect reciprocal line-graph TEP path is absent in the 2D lattice with an off-center site, there exists still a modified TEP line-graph path supporting STEPs and self-ODTEPs.

Finally, we discuss some physical phenomena and potential applications related to EPs, in particular the high-order TEPs and their evolution in NH line-graph lattices of this work. The singularity and topology of EPs in the parameter or momentum space give rise to rich physical phenomena, which have broad implications, especially in various artificial systems including microwave and optical cavities, photonic and acoustic lattices, etc. For example, the eigenvalue spectrum around doubly-degenerate EPs with deviation/perturbation  $\delta k$  is  $E \sim (\delta k)^{1/2}$ , which is in stark contrast to the common spectrum  $E \sim (\delta k)^1$  or  $E \sim (\delta k)^2$  around a degenerate point in Hermitian systems. Given that  $(\delta k)^{1/2} \gg (\delta k)^1 \gg (\delta k)^2$  for small  $|\delta k| \ll 1$ , the sensing response based on the perturbation away from an EP is greatly enhanced compared to that of Hermitian systems. One manifestation is the enhanced Sagnac effect (i.e. phase difference) between clockwise and counter-clockwise propagating light waves, which has been used to fabricate ultrasensitive gyroscope for the measurement of rotations [5, 6, 36, 37], and ultrasensitive optical microcavity for single-particle detection [38–40]. Furthermore, the sensitivity can be further boosted by higher-order EPs [8, 9] beyond the doubly degeneracy, such as the TEPs we studied here. Another interesting aspect of EPs is that it carries fractional charge, which is of general interest in entanglement of quantum states, relating to

**Table 1.** TEPs in 2D line-graph lattices with three sites having gain and loss.

Topology lattice	STEP ( $\pm 1/3$ )	ODTEP ( $\pm 2/3$ )	Self-orthogonal DETP ( $\pm 2/3$ )
Line-graph	✓	✓	—
Modified line-graph	✓	—	✓

fractional statistics. A doubly-degenerate EP is known to carry  $\pm 1/2$  charge, which produces a half-twisted vector-vortex beam with a half-charge polarization [1, 2, 41]. The EPs found here in the NH kagome (i.e. line-graph) lattice can have different degrees of degeneracy, and hence can carry different fractional charges including  $\pm 1/3$  and  $\pm 2/3$  charge etc., which are expected to result in different degrees of beam twisting and fractional polarization.

In general, EPs have been shown to support many underlying physical phenomena, including the unidirectional transmission or reflection [42–44], topological energy transfer between different modes [45, 46], loss-induced transparency [47], lasers with reversed pump dependence or single-mode operation [48–50]. Our findings of TEPs in the new line-graph lattices, having different fractional charges, and their intriguing evolutions will certainly enrich their physical phenomena and potential applications, especially in photonics, acoustics and elastic metamaterials.

## 4. Conclusion

In conclusion, 2D NH line-graph lattices with three sites having gain and loss are demonstrated to support three types of TEPs (see table 1). Interestingly, all the TEPs are located on a reciprocal line graph. STEPs with  $\pm 1/3$  topological charge move along the reciprocal lattice lines with varying gain and loss, while an intriguing form of ODTEPs with topological charge  $\pm 2/3$  appear at the reciprocal line-graph vertices by merging two STEPs. In contrast, the conventional self-ODTEP with three coalesced states appear in the 2D NH off-center line-graph lattices. These findings not only enrich the topological states in NH systems which may exhibit novel physical properties in realistic setups, but also point to new research directions to further link graph theory with topological physics, especially under non-equilibrium conditions.

## Acknowledgments

SM and HL thank financial support from the National Natural Science Foundation of China (Grant Nos. 91850120, 11774396, and 12147136), China Postdoctoral Science Foundation (Grant No. 2021M700163), and China Scholarship Council. FL is supported by US DOE-BES (Grant No. DE-FG02-04ER46148).

## Appendix A. Supplemental materials

Supplemental materials to this article can be found at <https://stacks.iop.org/NJP/23/123038/mmedia>.

## Data availability statement

The data that support the findings of this study are available upon reasonable request from the authors.

## ORCID iDs

Hang Liu  <https://orcid.org/0000-0001-6586-3040>

Sheng Meng  <https://orcid.org/0000-0002-1553-1432>

## References

- [1] Zhou H, Peng C, Yoon Y, Hsu C W, Nelson K A, Fu L, Joannopoulos J D, Soljačić M and Zhen B 2018 Observation of bulk Fermi arc and polarization half charge from paired exceptional points *Science* **359** 1009
- [2] Shen H, Zhen B and Fu L 2018 Topological band theory for non-Hermitian Hamiltonians *Phys. Rev. Lett.* **120** 146402
- [3] Leykam D, Bliokh K Y, Huang C, Chong Y D and Nori F 2017 Edge modes, degeneracies, and topological numbers in non-Hermitian systems *Phys. Rev. Lett.* **118** 040401
- [4] Miri M A and Alu A 2019 Exceptional points in optics and photonics *Science* **363** eaar7709

- [5] Hokmabadi M P, Schumer A, Christodoulides D N and Khajavikhan M 2019 Non-Hermitian ring laser gyroscopes with enhanced Sagnac sensitivity *Nature* **576** 70
- [6] Lai Y-H, Lu Y-K, Suh M-G, Yuan Z and Vahala K 2019 Observation of the exceptional-point-enhanced Sagnac effect *Nature* **576** 65
- [7] Zhang K L, Jin L and Song Z 2019 Helical resonant transport and purified amplification at an exceptional point *Phys. Rev. B* **100** 144301
- [8] Lin Z, Pick A, Lončar M and Rodriguez A W 2016 Enhanced spontaneous emission at third-order Dirac exceptional points in inverse-designed photonic crystals *Phys. Rev. Lett.* **117** 107402
- [9] Hodaei H, Hassan A U, Wittek S, Garcia-Gracia H, El-Ganainy R, Christodoulides D N and Khajavikhan M 2017 Enhanced sensitivity at higher-order exceptional points *Nature* **548** 187
- [10] Zhang G-Q and You J Q 2019 Higher-order exceptional point in a cavity magnonics system *Phys. Rev. B* **99** 054404
- [11] Schnabel J, Cartarius H, Main J, Wunner G and Heiss W D 2017 PT-symmetric waveguide system with evidence of a third-order exceptional point *Phys. Rev. A* **95** 053868
- [12] Mandal I and Bergholtz E J 2021 Symmetry and higher-order exceptional points *Phys. Rev. Lett.* **127** 186601
- [13] Delplace P, Yoshida T and Hatsugai Y 2021 Symmetry-protected multifold exceptional points and their topological characterization *Phys. Rev. Lett.* **127** 186602
- [14] Zhen B, Hsu C W, Igarashi Y, Lu L, Kaminer I, Pick A, Chua S-L, Joannopoulos J D and Soljačić M 2015 Spawning rings of exceptional points out of Dirac cones *Nature* **525** 354
- [15] Cerjan A, Raman A and Fan S 2016 Exceptional contours and band structure design in parity-time symmetric photonic crystals *Phys. Rev. Lett.* **116** 203902
- [16] Xu Y, Wang S T and Duan L M 2017 Weyl exceptional rings in a three-dimensional dissipative cold atomic gas *Phys. Rev. Lett.* **118** 045701
- [17] Cerjan A, Huang S, Wang M, Chen K P, Chong Y and Rechtsman M C 2019 Experimental realization of a Weyl exceptional ring *Nat. Photon.* **13** 623
- [18] Wang H, Ruan J and Zhang H 2019 Non-Hermitian nodal-line semimetals with an anomalous bulk-boundary correspondence *Phys. Rev. B* **99** 075130
- [19] Yang Z and Hu J 2019 Non-Hermitian Hopf-link exceptional line semimetals *Phys. Rev. B* **99** 081102(R)
- [20] Carlström J, Stålhammar M, Budich J C and Bergholtz E J 2019 Knotted non-Hermitian metals *Phys. Rev. B* **99** 161115(R)
- [21] Okugawa R and Yokoyama T 2019 Topological exceptional surfaces in non-Hermitian systems with parity-time and parity-particle-hole symmetries *Phys. Rev. B* **99** 041202(R)
- [22] Szameit A, Rechtsman M C, Bahat-Treidel O and Segev M 2011 PT-symmetry in honeycomb photonic lattices *Phys. Rev. A* **84** 021806(R)
- [23] Harari G, Bandres M A, Lumer Y, Rechtsman M C, Chong Y D, Khajavikhan M, Christodoulides D N and Segev M 2018 Topological insulator laser: theory *Science* **359** eaar4003
- [24] Bandres M A, Wittek S, Harari G, Parto M, Ren J, Segev M, Christodoulides D N and Khajavikhan M 2018 Topological insulator laser: experiments *Science* **359** eaar4005
- [25] Weimann S, Kremer M, Plotnik Y, Lumer Y, Nolte S, Makris K G, Segev M, Rechtsman M C and Szameit A 2017 Topologically protected bound states in photonic parity-time-symmetric crystals *Nat. Mater.* **16** 433
- [26] Yao S and Wang Z 2018 Edge states and topological invariants of non-Hermitian systems *Phys. Rev. Lett.* **121** 086803
- [27] Liu T, Zhang Y R, Ai Q, Gong Z, Kawabata K, Ueda M and Nori F 2019 Second-order topological phases in non-Hermitian systems *Phys. Rev. Lett.* **122** 076801
- [28] Zhang Z, Rosendo López M, Cheng Y, Liu X and Christensen J 2019 Non-Hermitian sonic second-order topological insulator *Phys. Rev. Lett.* **122** 195501
- [29] Mielke A 1991 Ferromagnetic ground states for the Hubbard model on line graphs *J. Phys. A: Math. Gen.* **24** L73
- [30] Mielke A 1991 Ferromagnetism in the Hubbard model on line graphs and further considerations *J. Phys. A: Math. Gen.* **24** 3311
- [31] Mielke A 1992 Exact ground states for the Hubbard model on the kagome lattice *J. Phys. A: Math. Gen.* **25** 4335
- [32] Miyahara S, Kusuta S and Furukawa N 2007 BCS theory on a flat band lattice *Physica C* **460–462** 1145
- [33] Liu Z, Liu F and Wu Y-S 2014 Exotic electronic states in the world of flat bands: from theory to material *Chin. Phys. B* **23** 077308
- [34] Wu C, Bergman D, Balents L and Das Sarma S 2007 Flat bands and Wigner crystallization in the honeycomb optical lattice *Phys. Rev. Lett.* **99** 070401
- [35] Zheng M C, Christodoulides D N, Fleischmann R and Kottos T 2010 PT optical lattices and universality in beam dynamics *Phys. Rev. A* **82** 010103(R)
- [36] Ren J, Hodaei H, Harari G, Hassan A U, Chow W, Soltani M, Christodoulides D and Khajavikhan M 2017 Ultrasensitive micro-scale parity-time-symmetric ring laser gyroscope *Opt. Lett.* **42** 1556
- [37] Sunada S 2017 Large Sagnac frequency splitting in a ring resonator operating at an exceptional point *Phys. Rev. A* **96** 033842
- [38] Wiersig J 2014 Enhancing the sensitivity of frequency and energy splitting detection by using exceptional points: application to microcavity sensors for single-particle detection *Phys. Rev. Lett.* **112** 203901
- [39] Liu Z-P et al 2016 Metrology with PT-symmetric cavities: enhanced sensitivity near the PT-phase transition *Phys. Rev. Lett.* **117** 110802
- [40] Chen W, Özdemir S K, Zhao G, Wiersig J and Yang L 2017 Exceptional points enhance sensing in an optical microcavity *Nature* **548** 192
- [41] Midya B, Zhao H and Feng L 2018 Non-Hermitian photonics promises exceptional topology of light *Nat. Commun.* **9** 2674
- [42] Regensburger A, Bersch C, Miri M-A, Onishchukov G, Christodoulides D N and Peschel U 2012 Parity-time synthetic photonic lattices *Nature* **488** 167
- [43] Lin Z, Ramezani H, Eichelkraut T, Kottos T, Cao H and Christodoulides D N 2011 Unidirectional invisibility induced by PT-symmetric periodic structures *Phys. Rev. Lett.* **106** 213901
- [44] Peng B et al 2014 Parity-time-symmetric whispering-gallery microcavities *Nat. Phys.* **10** 394
- [45] Doppler J et al 2016 Dynamically encircling an exceptional point for asymmetric mode switching *Nature* **537** 76
- [46] Xu H, Mason D, Jiang L and Harris J G E 2016 Topological energy transfer in an optomechanical system with exceptional points *Nature* **537** 80
- [47] Guo A, Salamo G J, Duchesne D, Morandotti R, Volatier-Ravat M, Aimez V, Siviloglou G A and Christodoulides D N 2009 Observation of PT-symmetry breaking in complex optical potentials *Phys. Rev. Lett.* **103** 093902

- [48] Liertzer M, Ge L, Cerjan A, Stone A D, Türeci H E and Rotter S 2012 Pump-induced exceptional points in lasers *Phys. Rev. Lett.* [108 173901](#)
- [49] Hodaei H, Miri M-A, Heinrich M, Christodoulides D N and Khajavikhan M 2014 Parity-time-symmetric microring lasers *Science* [346 975](#)
- [50] Feng L, Wong Z J, Ma R-M, Wang Y and Zhang X 2014 Single-mode laser by parity-time symmetry breaking *Science* [346 972](#)